

# Measuring the Angular Momentum of a Neutron Using Earth’s Rotation

Niels Geerits\* and Stephan Sponar

*Atominstytut, Technische Universität Wien, Stadionallee 2, 1020 Vienna, Austria*

Kyle E. Steffen and William M. Snow

*Centre for Exploration of Energy and Matter, Indiana University, Bloomington, 47408, US*

Steven R. Parnell, Giacomo Mauri, Gregory N. Smith, and Robert M. Dalgliesh

*ISIS, Rutherford Appleton Laboratory, Chilton, Oxfordshire, OX11 0QX, UK*

Victor de Haan

*BonPhysics Research and Investigations BV, Laan van Heemstede 38, 3297AJ Puttershoek, The Netherlands*

(Dated: July 22, 2024)

A coupling between Earth’s rotation and orbital angular momentum (OAM), known as the Sagnac effect, is observed in entangled neutrons produced using a spin echo interferometer. After correction for instrument systematics the measured coupling is within 5% of theory, with an uncertainty of 7.2%. The OAM in our setup is transverse to the propagation direction and scales linearly with neutron wavelength (4 Å– 12.75 Å), so the Sagnac coupling can be varied without mechanically rotating the device, which avoids systematic errors present in previous experiments. The detected transverse OAM of our beam corresponds to  $4098 \pm 295 \hbar \text{Å}^{-1}$ ,  $10^5$  times lower than in previous neutron experiments. This demonstrates the feasibility of using the Sagnac effect to definitively measure neutron OAM and paves the way towards a future observation of the quantum Sagnac effect.

## INTRODUCTION

In non-inertial frames of reference the laws of nature may appear to work differently, due to additional quasi-forces that arise as a result of the non-uniform motion of the reference frame. George Sagnac’s 1913 experiment is a famous example of such an effect. In an attempt to prove the existence of an ether, Sagnac observed a phase shift in his interferometer which depended on the direction in which the interferometer was rotated [1]. The Sagnac effect manifests as an apparent coupling between the rotation frequency of the observer and the angular momentum of the test particle. The famous 1925 experiment by Michelson, Gale and Pearson, was able to observe this coupling in a very large optical interferometer due to the Earth’s rotation [2]. Since Sagnac and Michelson made their observations with light, the experimental question remained whether or not matter waves also experience a pseudo-potential in a rotating frame. In 1979, Werner, Staudenmann, and Colella managed to demonstrate that neutrons traversing a rotating interferometer also experience a phase shift proportional to the inner product between the rotation frequency,  $\Omega$  and the Orbital Angular Momentum (OAM),  $L$  spanned by the neutron’s motion in the interferometer ( $\Omega \cdot L$ ) [3]. The rotation of the interferometer was realized by the natural rotation of the earth, as was the case in the 1925 Michelson/Gale/Pearson experiment. In addition to neutrons, the Sagnac effect has also been observed in other matter waves, such as electrons [4] and atoms [5]. In 1988 Mashhoon demonstrated that this

effect extends to the intrinsic spin angular momentum of particles as well as their orbital angular momentum [6]. Recently the Mashhoon effect has been observed in neutron polarimetry [7] and in neutron interferometry [8]. In these cases the rotating frame was realized by creating a rotating magnetic field in the laboratory frame of the interferometer which, for the projective measurement of the neutron spin employed in the apparatus, can be shown to be equivalent to observing the neutron spin in a rotating frame of reference.

In parallel with this work on the Mashhoon effect, neutron researchers started to produce neutrons with quantized OAM [9–12]. Quantum mechanical OAM reduces to the usual definition of angular momentum in the classical limit  $\hat{L} = \hat{r} \times \hat{p}$ , but distinguishes itself by possessing discrete integer multiples of  $\hbar$  upon measurement. OAM can be considered to be “intrinsic” if the expectation value of  $\hat{L}$  is spatially translation invariant [13–15]. Detection of neutron OAM remains difficult and is the subject of debate and discussion in the scientific literature [16, 17]. Current proposed methods are based on neutron scattering and absorption [18–20]. The simplicity of the effective potential created by the Sagnac effect, which contains only the OAM operator and an external quantity, could prove useful for the definitive detection of neutron OAM. The neutrons used in the 1975 experiment possessed OAM with respect to the center of the interferometer on the order of  $10^9 \hbar$ . This OAM was detected by the rotation of the earth. In this paper we improve the angular momentum sensitivity for neutron OAM been through the Sagnac

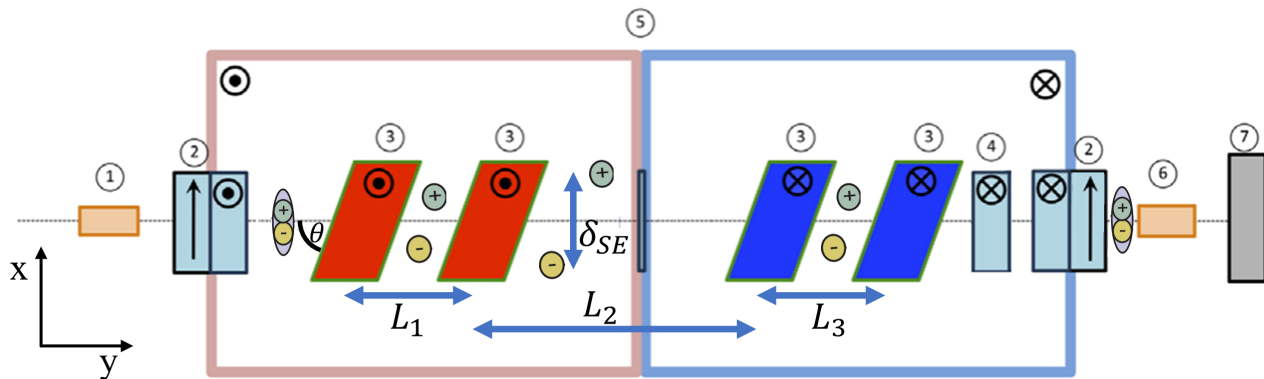


FIG. 1. Schematic of the Larmor neutron spin echo interferometer, the propagation of the + and - spin through the device and the neutron optical components: (1) polarizer (2) adiabatic  $\pi/2$  rotator (v-coil), (3) RF spin flipper with tilted field region, (4) ramped  $\pi/2$  rotator (5) guide field, (6) spin analyzer and (7) detector.

effect by 5 orders of magnitude, measuring  $\approx 10^4$  units of  $\hbar$ . This 5 orders of magnitude improvement in sensitivity marks an important step towards observation of the quantized Sagnac effect. In optics this quantized Sagnac effect has been observed using spinning Dove prisms [21]. The observation of a quantized energy shift from the Sagnac effect is an attractive method to resolve quantized OAM states in neutrons. We report on an experimental observation of the Sagnac effect in a neutron interferometer which uses microscopic path separation on the order of the transverse coherence of the neutron ( $0.001\mu m - 100\mu m$ ) [22–24]. In addition we demonstrate that the Sagnac effect provides a good method for a basis to definitively detect the OAM of a particle. Our experiment was carried out on the Larmor instrument at the ISIS pulsed neutron source. Larmor is a neutron spin echo type interferometer [25], which employs shaped RF spin flippers to induce horizontal spin and energy dependent path separation [26, 27]. As a result the spin, energy and path degrees of freedom of the neutron are entangled [28, 29].

## THEORY

In a rotating frame of reference, particles experience a pseudo potential proportional to the rotation rate of the frame and the OAM possessed by the particle around the axis of rotation

$$\hat{V} \propto \Omega \cdot \hat{L} \quad (1)$$

with  $\hat{L}$  the OAM operator  $\hat{L} = \hat{r} \times \hat{p}$ . For our setup (see figure 1), it can be shown that for spin echo lengths (i.e. splitting distances)  $\delta_{SE}$ , much larger than the transverse beam coherence [22, 24], the expected OAM Eigenvalue transverse to the propagation direction is

$$\ell_{\pm} = \pm \frac{\delta_{SE}|k|}{2}, \quad (2)$$

where the sign is determined by whether the neutron passes the rotation axis left or right and  $|k|$  is the wavenumber. It follows that the two path states, defined by the spin echo length  $\delta_{SE}$  can also be described by two OAM states. Thus, for the purposes of this experiment, we describe our state not as spin-path entangled, but as spin-orbit entangled, such that the state in the center of the interferometer can be described as

$$|\psi\rangle = |\ell_{+}\rangle |\uparrow\rangle + e^{i\phi} |\ell_{-}\rangle |\downarrow\rangle \quad (3)$$

with  $\phi$  the phase difference between the two entangled states. The precession frequency between the two states due to the Sagnac effect follows from eq. 1 and 2 and is given by

$$\delta\omega_s = [\ell_{+} - \ell_{-}]\Omega \sin(\Lambda) \quad (4)$$

with  $\Lambda$  the latitude of the interferometer. Integrating this precession frequency over the length of the instrument leads to the Sagnac phase shift

$$\delta\phi_s = \int dt \delta\omega_s = \frac{m\Omega\Delta\ell}{\hbar|k|} \sin(\Lambda)[L_1 + L_3 + 2L_2], \quad (5)$$

which can be reduced to the result shown in [3, 30], for a horizontal interferometer.

$$\delta\phi_s = \frac{2mA\Omega}{\hbar} \sin(\Lambda) \quad (6)$$

with  $A$  the area spanned by the two paths of the interferometer. The area, illustrated in figure 1, is given by

$$A = \delta_{SE} \left[ \frac{L_1 + L_3}{2} + L_2 \right]. \quad (7)$$

As will be shown in the next section the spin echo length,  $\delta_{SE}$  is proportional to wavelength squared in spin echo interferometers. Hence to vary the area of the interferometer and therefore strength of the Sagnac

effect, we may simply vary the wavelength of incident neutrons, whereas the 1979 perfect crystal experiment required physical rotation of the interferometer, which may induce systematic errors.

In equation 5 we put the acquired Sagnac phase in a form that shows that one can extract the difference between the quantum numbers for two OAM states, assuming instrument parameters and the rotation rate are well known. Hence, using the Sagnac effect can be a good relative measure to determine the OAM of a beam.

## METHODS

Our measurements were carried out on the Larmor instrument at the ISIS pulsed neutron source [31]. Larmor is a SANS instrument with a versatile neutron resonant spin echo toolbox, based on four gradient radio frequency spin flippers with shaped poleshoes, capable of performing inelastic techniques such as Modulated Intensity Emerging from Zero Effort (MIEZE) [27] and Spin Echo (Modulated) Small Angle Neutron Scattering (SE(M)SANS) [28, 29, 32, 33]. Our experiment makes use of the SESANS mode of the instrument, which employs magnetic refraction from a tilted field region to induce spin dependent spatial splitting and a second oppositely polarized field region to recombine the two split states (see figure 1). The path separation, also known as the spin echo length is proportional to the wavelength squared

$$\delta_{SE} = \frac{m\gamma B_0 L_1 \cot(\theta)}{2\pi^2 \hbar} \lambda^2 = c_{SE} \lambda^2 \quad (8)$$

with  $\gamma$  the gyromagnetic ratio of the neutron,  $\lambda$  the neutron wavelength,  $m$  the neutron mass,  $B_0$  the magnitude of the static magnetic field inside the RF flippers and  $\theta$ , the angle between the incident beam and the magnetic field region. The constant  $c_{SE}$  which summarizes all instrument parameters and constants, is called the spin echo constant. This interferometric technique has previously been used to revisit the Colella-Overhauser-Werner experiment [30], put limits on exotic spin-gravity couplings [34] and measure Bell inequalities with neutrons [28, 29].

Since Larmor uses spin dependent refraction to realise the interferometer, the path and spin states of the neutron are coupled (i.e. mode entangled). Hence any path dependent phase shift is projected onto the spin and vice-versa. As pointed out previously the path and OAM degree of freedom are related, hence the path state and also path phases, may also be described as orbit states/phases. In SESANS the spin is usually prepared, along the x-axis, orthogonal to the beam propagation and  $B_0$  direction. The expectation value of the spin, also called polarisation, is usually also measured along the

x-direciton, leading to a polarisation of

$$P_x = P_0 \cos(\Delta\phi(\lambda)) \quad (9)$$

with  $P_0 = \sqrt{P_x^2 + P_y^2 + P_z^2}$  and  $\Delta\phi(\lambda)$  a polynomial in  $\lambda$

$$\Delta\phi(\lambda) = a_0 + a_1\lambda + a_2\lambda^2 + O(\lambda^3). \quad (10)$$

One may independently control the  $a_0$  term by means of a ramped precession field, with  $B(t) \propto 1/t$ , which ensures that the spin of each wavelength on a ToF source is rotated by the same angle [35, 36]. By setting  $a_0$  equal to  $\pi/2$  we effectively change the measurement direction to along the y-axis, the propagation direction. Hence the measured polarisation becomes

$$P_y = P_0 \sin(\Delta\phi'(\lambda)), \quad (11)$$

which for small  $\Delta\phi'$  may be linearized. To remove the scaling factor  $P_0$ , we may normalise  $P_y$  by  $P_x$ . This normalized polarization still has a simple and accurate linearization for small  $\Delta\phi$

$$\frac{P_y}{P_x} \approx \epsilon + a_1\lambda + a_2\lambda^2 \quad (12)$$

with  $\epsilon$  any imprecision in the quality of the  $\pi/2$  rotation provided by the ramped precession field. We can estimate the second order parameter, due to the Sagnac effect using equations 6 and 8

$$a_2 = c_{SE} \frac{m\Omega}{\hbar} \sin(\Lambda)[L_1 + L_3 + 2L_2]. \quad (13)$$

However additional perturbations arising from imperfections in the instrument can occur which can affect the magnitude of the second order term. Most notably a slight change in the precession plane can occur if an imperfect spin optical component introduces an unintended low probability spin flip. Components that may be suspected to introduce such an effect are primarily those which use adiabatic field changes to affect a spin rotation, for example v-coils (item 2 in figure 1) and adiabatic RF flippers (item 3 in figure 1), since adiabatic spin flip probabilities in both of these components can be described as

$$\rho \approx A_i \lambda^2 \cos^2(k_i \lambda + \alpha) \quad (14)$$

assuming only slight imperfection [37, 38] (i.e. low spin flip probability). As a result the precession plane will appear to oscillate with an amplitude proportional to  $\lambda^2$  and in addition this effect will produce an aberration on  $a_2$ , since the  $\cos^2$  component in equation 14 produces a constant offset. This offset can of course be isolated and subtracted from  $a_2$ , by measuring the amplitude of the precession plane oscillation. Since this effect is small it has not been relevant to measurements conducted with

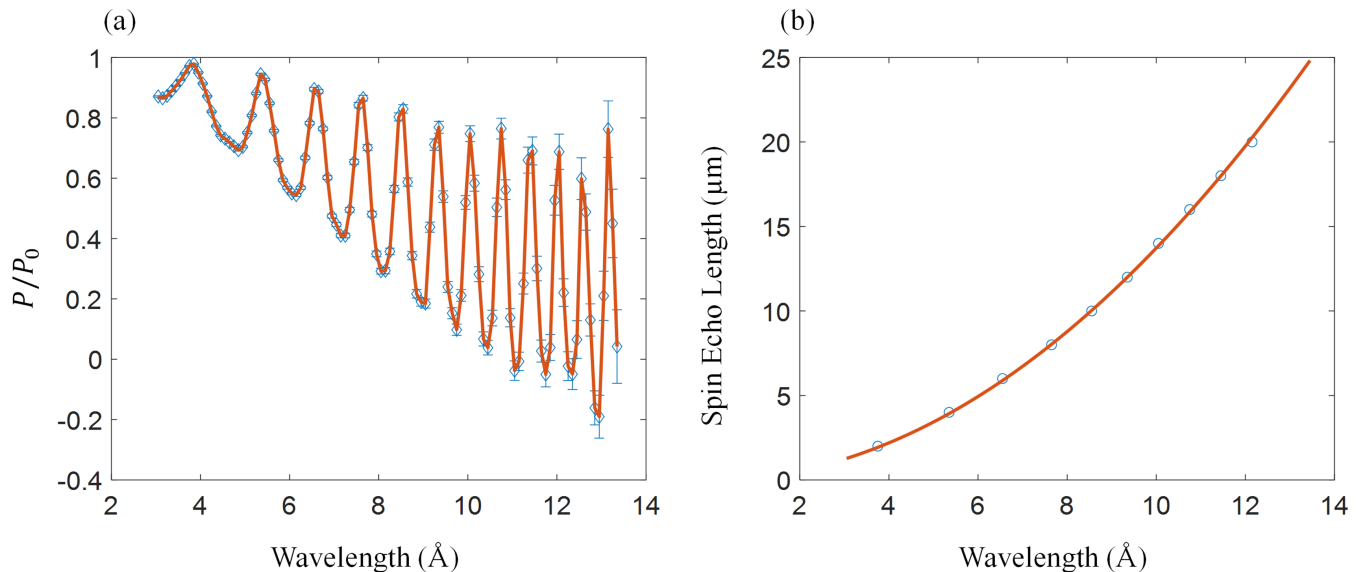


FIG. 2. Calibration curves of the instrument produced using a 2  $\mu\text{m}$  period silicon grating. (a) Plot of the normalized spin-echo polarization against wavelength. The  $n^{\text{th}}$  peak corresponds to a spin echo length equal to  $n$  times the grating period. The wavelength and corresponding spin echo length is extracted and plotted in the next panel (b). The quadratic fit is drawn in red.

Larmor before, however our experiment has sufficient sensitivity to uncover this systematic.

Measurements of the Sagnac phase were conducted using a pole shoe angle of  $\theta = 40$  degrees and at an RF frequency of 2 MHz corresponding to a magnetic field strength of 68.6 mT. These consisted of polarization measurements with the ramped  $\pi/2$  rotator turned off and on with both polarities (corresponding to a  $\pi/2$  or  $-\pi/2$  rotation). In addition with the ramped  $\pi/2$  rotator turned off a calibration measurement was carried out, in which a 2 micron silicon grating was inserted into the sample position of the instrument. The resulting correlation function, shown in figure 2 (a), allows us to experimentally determine the proportionality constant between the spin echo length and the wavelength squared, which is essential to estimate  $a_2$ . Since the  $n^{\text{th}}$  peak in figure 2 (a) corresponds to a spin echo length of  $n$  times the grating period, one can extract the relationship between spin echo length and wavelength, shown in figure 2 (b). By applying a quadratic fit one finds the spin echo constant,  $c_{SE}$ , to be equal to  $0.137 \mu\text{m}\text{\AA}^{-2}$ . Using this and equation 13 it follows that for the instrument settings used in this experiment the Sagnac constant  $a_2$ , should be equal to  $-1.15 \times 10^{-3} \text{\AA}^{-2}$ . Equations 2 or 5, show that the difference between OAM states scales linearly with  $\lambda$  (i.e.  $\delta\ell = c_{OAM}\lambda$ ). Using equation 5 we can express  $c_{OAM}$  in terms of  $a_2$

$$c_{OAM} = \frac{2\pi\hbar a_2}{m\Omega \sin(\Lambda)[L_1 + L_3 + 2L_2]} \quad (15)$$

which for our estimated value of  $a_2$  is equal to  $-8.62 \times$

	$a_2$ ( $\text{\AA}^{-2}$ ) $\times 10^3$	$ A_1 $ ( $\text{\AA}^{-2}$ ) $\times 10^5$	$ A_2 $ ( $\text{\AA}^{-2}$ ) $\times 10^5$
$P_+$	$-0.891 \pm 0.0853$	$14.4 \pm 2.31$	$8.22 \pm 2.24$
$P_-$	$0.898 \pm 0.0739$	$8.88 \pm 1.85$	$6.23 \pm 1.83$

$$a_2^S = (-0.894 \pm 0.0564) \times 10^{-3} \text{\AA}^{-2} \quad c_{OAM} = -6767 \pm 427 \text{\AA}^{-1}$$

TABLE I. Table containing the second order fit parameters,  $a_2$  and their respective standard deviations, for both coil polarities and the amplitudes of the oscillations found in the data with their respective errors. The final estimate for the second order parameter due to the Sagnac effect,  $a_2^S$ , which is calculated using equation 16, is shown at the bottom, in addition to the OAM proportionality constant (see equation 15).

$10^3 \text{\AA}^{-1}$ . Since according to equation 2  $\ell_+$  and  $\ell_-$  are equal in magnitude it follows that the OAM of each state scales with  $\ell_{\pm} = \pm \frac{1}{2} c_{OAM} \lambda$ .

## RESULTS

The normalized polarization, for the positive  $\pi/2$  rotator polarity, is shown in figure 3 (a). This represents a typical spin-echo curve obtained from this experiment. It is clear that the raw data contains oscillations which increase in amplitude with wavelength squared, analogous to the precession plane oscillation described in the previous section (see eq. 14). By subtracting a quadratic fit from the data and dividing the result by  $\lambda^2$ , the oscillations can be isolated (see figure 3 (b)). It can be shown that the aberration consists of two oscillations with frequencies  $k_2 \approx 2k_1$ . As pointed out previously it is important to

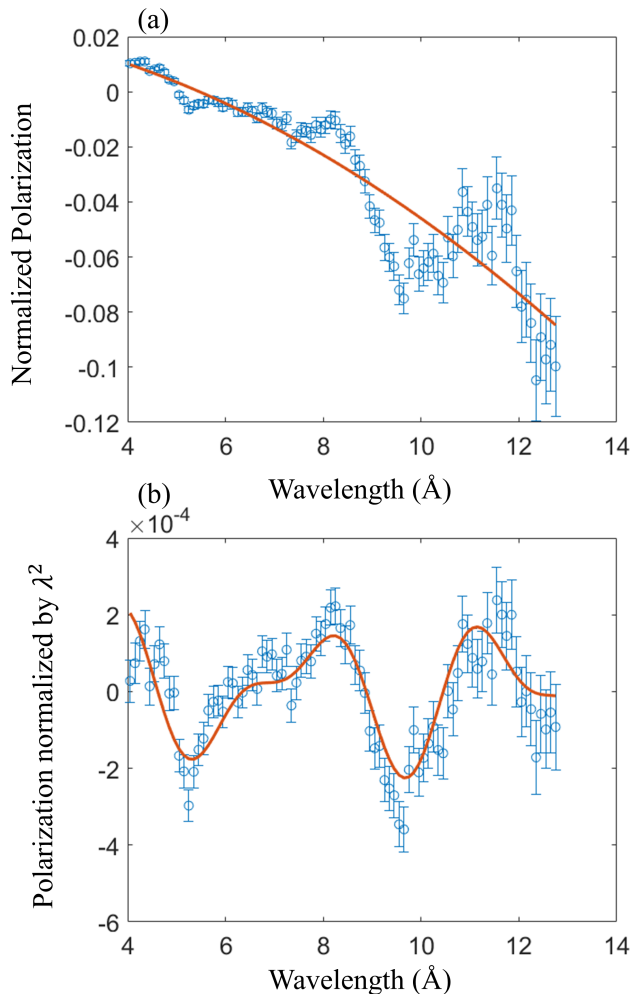


FIG. 3. (a) Typical normalized polarization for the 40 degree polehoe setting, in which the Sagnac phase shift is expected (blue). A quadratic fit is shown in red. The quadratic fit can be subtracted from the data to isolate the oscillations (b) Since the amplitude of the oscillations scale with wavelength squared, we divide these by  $\lambda^2$ . A fit consisting of two sines is shown in red.

correct for these oscillations, since in addition to improving the overall fit quality, the amplitude information is necessary to correct for a systematic error coming from imperfections of the instrument, hence both amplitudes are listed in table I. The data is corrected by fitting two sine waves to the oscillations and subtracting said fit multiplied by  $\lambda^2$  from the data. The corrected data for both  $\pi/2$  coil settings is shown in figure 4. Quadratic fits using a weighted least squares method are applied to the corrected data. The weights are given by the inverted variance. The second order fit parameters are illustrated in table I. The first estimate for the second order parameter  $a_2^S$ , due to the Sagnac effect is obtained

using the following

$$a_2^S = \frac{a_2^+ - a_2^-}{2} \quad (16)$$

Alternatively the corrected data may be aggregated according to a similar formula

$$P_S = \frac{P_+ - P_-}{2} \quad (17)$$

and a weighted least squares quadratic fit is applied to this result.  $P_S$  is shown in figure 5. The resulting second order fit parameter is  $(-0.899 \pm 0.0631) \times 10^{-3}$ , which is in good agreement with the value  $a_2^S$  shown in table I. For comparison figure 5 contains a fit in green which uses the theoretically exact value for the second order parameter, while the zeroth and first order coefficients are determined via least squares regression.

## DISCUSSION

Figure 5 indicates a good agreement between our calculated Sagnac parameter of  $-1.15 \times 10^{-3} \text{Å}^{-2}$  and the measured parameter, however the exact fit parameters shown in table I, indicate that for a single  $\pi/2$  rotator polarity, the measured value differs from our calculation by roughly  $3\sigma$ . Furthermore the averaged fit parameter  $a_2^S$ , differs from theory by  $4.3\sigma$ , indicating a high likelihood of a systematic perturbation. In this section we correct this perturbation to the second order fit parameter, assuming it is caused by imperfections in the adiabatic spin optical components. Both the oscillations shown in figure 3 and the large  $\propto 4\sigma$  deviation between data indicate that such imperfections are likely. As indicated earlier at low efficiencies adiabatic spin flip probabilities scale with  $\lambda^2$ , consistent with our observation. Therefore we postulate that the oscillations shown in figure 3 (b) arise due to an oscillation of the precession plane of the form

$$P = 2\lambda^2[|A_1| \cos^2(k_1\lambda + \phi_1) + |A_2| \cos^2(k_2\lambda + \phi_2)] \quad (18)$$

similar to equation 14, which introduces a systematic to the second order fit parameter of  $\pm[|A_1| + |A_2|]$ . Where the sign is determine by the polarity of the  $\pi/2$  rotator. The corrected second order parameters,  $\bar{a}_2$ , using the amplitudes shown in table I are shown in the table II. After applying this correction the average estimated second order parameter due to the Sagnac effect is  $(-1.083 \pm 0.078) \times 10^{-3}$ , which is within  $1\sigma$  of the expected theoretical value. This corresponds to an OAM proportionality constant of  $-8197 \pm 590$  units of  $\hbar/\text{Å}$  according to equation 15. From this the OAM Eigenvalues  $\ell_{\pm}$  of the two path states can be extracted:  $\ell_{\pm} = \pm 4098 \pm 295 \hbar/\text{Å} \cdot \lambda$ . This can be compared to the results of our calibration measurement (figure 2), which, based on equation 2, allows us to estimate the OAM

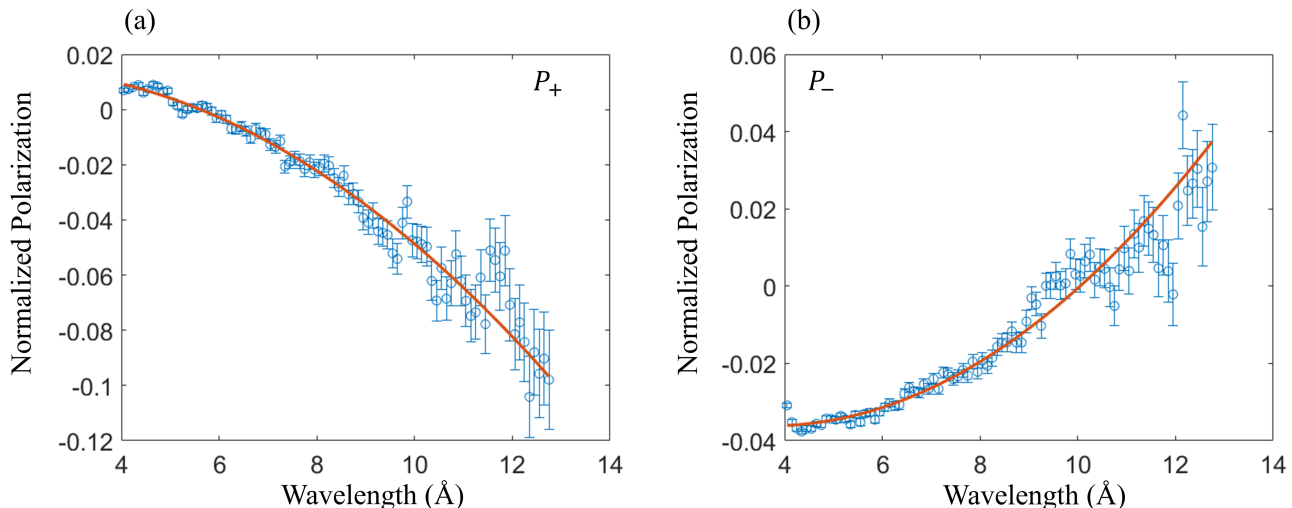


FIG. 4. Plots of the normalized and corrected polarization in blue for (a) positive polarity and (b) negative  $\pi/2$  rotator polarity. The quadratic fits are plotted in red. The errorbar introduced by subtracting the sinusoidal fit is negligible.

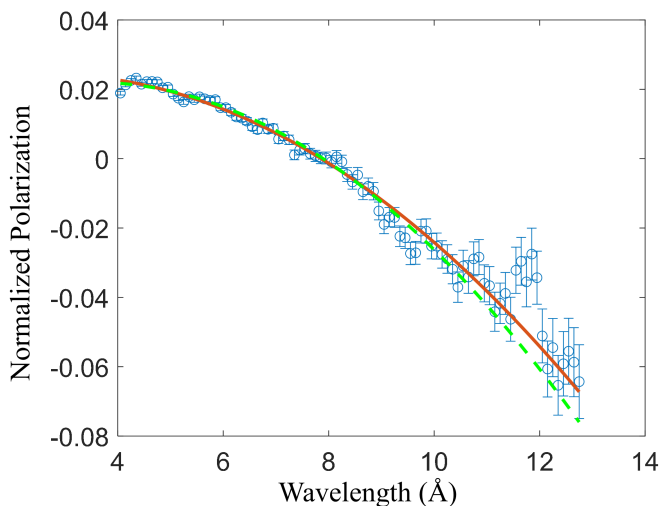


FIG. 5. Averaged normalized polarization of all data, according to equation 17, shown in blue. The quadratic fit is shown as a red solid line. While a fit containing the exact theoretical expectation value for the second order term due to the Sagnac effect is shown as a green dashed line.

	$\bar{P}_+$	$\bar{P}_-$	$\frac{P_+ - P_-}{2}$
$\bar{a}_2(\text{\AA}^{-2}) \times 10^3$	$-1.117 \pm 0.121$	$1.049 \pm 0.098$	$-1.083 \pm 0.078$
$\bar{c}_{OAM}(\text{\AA}^{-1})$	$-8454 \pm 916$	$7940 \pm 742$	$-8197 \pm 590$

TABLE II. Corrected estimates for the second order parameter due to the Sagnac effect,  $\bar{a}_2$ , and their respective errors for both  $\pi/2$  coil polarities and their average, in addition to the OAM proportionality constant,  $\bar{c}_{OAM}$  for each setting. For comparison our theoretical estimate for  $a_2$  is  $-1.15 \times 10^{-3} \text{\AA}^{-2}$  and for  $c_{OAM}$  is  $-8.62 \times 10^3 \text{\AA}^{-1}$

Eigenvalue  $\ell_{\pm} = \pm 4310$ , which is within  $1\sigma$  of the estimate achieved using the Sagnac effect. We conclude that the Sagnac effect represents the first definitive detection of transverse neutron OAM, since it depends only on the projection of the OAM on the axis of rotation (equation 1), meaning that OAM must be present to explain a non-zero result. Further, answering criticism raised in [16], against the first experiments with neutron beam OAM [9], we propose to use OAM-rotation coupling to definitively detect longitudinal OAM. The sensitivity of this method, using the earth's rotation, is sufficient for detecting large quanta of OAM  $|\ell| > 10^3$ , however it can be significantly improved by increasing the rotation frequency. A higher effective rotation frequency can be achieved by inserting a rotating Dove mirror (see for example [11, 21, 39]) in the center of the instrument. A low rotation frequency of 1 Hz, would increase sensitivity by  $10^5$ , compared to earth's rotation. This method would increase  $a_2$  and  $c_{OAM}$ , such that the systematic induced by the slight oscillations of the precession plane, becomes insignificant. The Dove mirror could be made compact, albeit monochromatic, if mosaic crystals are used to produce reflections. We postulate that such devices will play an important role in neutron OAM optics for OAM manipulation and detection, since as opposed to the scattering methods reported on in [18–20], the efficiency of a Sagnac based method is independent of other attributes of the neutron wavepacket such as coherence length. As pointed out in previous sections our technique uses spin-orbit entanglement to imprint OAM dependent phases on the spin (see for example eq. 3) and to characterize these phases by measuring the spin projection. This is somewhat analogous to the entangled optical interferometer reported on in [40], which makes

use of inter-particle entanglement, while we report on intra-particle or mode entanglement. The  $1\sigma$  precision achieved in our experiment corresponds to a rotational sensitivity of  $5.1\mu\text{rad} \cdot \text{s}^{-1}$ , similar to what is reported in [40], which to our our knowledge is the most sensitive measurement of the Sagnac effect using entanglement.

### ACKNOWLEDGMENTS

N. G. and S. S. acknowledge funding from the Austrian science fund (FWF), Project No. P34239, in addition N. G. and W. M. S. are supported by the US Department of Energy (DOE) grant DE-SC0023695. W. M. S. and K. S. acknowledge support from the US National Science Foundation (NSF) grant PHY-2209481 and the Indiana University Center for Spacetime Symmetries. The authors extend their gratitude to Gøran Nilsen for supplying the ramped  $\pi/2$  flipper. Experiments at the ISIS Neutron and Muon Source were supported by a beamtime allocation RB2410116 [31] from the Science and Technology Facilities Council.

### REFERENCES

\* niels.geerits@tuwien.ac.at

- [1] M. G. Sagnac. The demonstration of the luminiferous aether by an interferometer in uniform rotation. *Comptes Rendus*, 157:708,1410, 1913.
- [2] A. A. Michelson, H. G. Gale, and F. Pearson. The effect of the earth's rotation on the velocity of light, ii. *AstroPhysical Journal*, 61:140, 1925.
- [3] S. A. Werner, J. L. Staudenmann, and R. Colella. Effect of earth's rotation on the quantum mechanical phase of the neutron. *Phys. Rev. Lett.*, 42:1103–1106, 1979.
- [4] Franz Hasselbach and Marc Nicklaus. Sagnac experiment with electrons: Observation of the rotational phase shift of electron waves in vacuum. *Phys. Rev. A*, 48:143–151, 1993.
- [5] F. Riehle, Th. Kisters, A. Witte, J. Helmcke, and Ch. J. Bordé. Optical ramsey spectroscopy in a rotating frame: Sagnac effect in a matter-wave interferometer. *Phys. Rev. Lett.*, 67:117, 1991.
- [6] Bahram Mashhoon. Neutron interferometry in a rotating frame of reference. *Physical Review Letters*, 61:2639–2642, 1988.
- [7] Bülent Demirel, Stephan Sponar, and Yuji Hasegawa. Measurement of the spin-rotation coupling in neutron polarimetry. *New Journal of Physics*, 17:023065, 2015.
- [8] Armin Danner, Bülent Demirel, Wenzel Kersten, Hartmut Lemmel, Richard Wagner, Stephan Sponar, and Yuji Hasegawa. Spin-rotation coupling observed in neutron interferometry. *npj Quantum Information*, 6(23), 2020.
- [9] Charles W. Clark, Roman Barankov, Michael G. Huber, Muhammad Arif, David G. Cory, and Dmitry A. Pushin. Controlling neutron orbital angular momentum. *Nature*, 525:504–506, 2015.
- [10] D. Sarenac, C. Kapahi, W. Chen, C. W. Clark, D. G. Cory, M. G. Huber, I. Taminiau, K. Zhernenkov, and D. A. Pushin. Generation and detection of spin-orbit coupled neutron beams. *PNAS*, 116:20328–20332, 2019.
- [11] N. Geerits and S. Sponar. Twisting neutral particles with electric fields. *Phys. Rev. A*, 103:022205, 2021.
- [12] Dusan Sarenac, Melissa E. Henderson, Huseyin Ekinci, Charles W. Clark, David G. Cory, Lisa DeBeer-Schmitt, Michael G. Huber, Connor Kapahi, and Dmitry A. Pushin. Experimental realization of neutron helical waves. *Sci. Adv.*, 8:eadd2002, 2022.
- [13] Michael V. Berry. Paraxial beams of spinning light. *Proc. SPIE*, 3487:6–11, 1998.
- [14] A. T. O'Neil, I. MacVicar, L. Allen, and M. J. Padgett. Intrinsic and extrinsic nature of the orbital angular momentum of a light beam. *Physical Review Letters*, 88:053601, 2002.
- [15] N. Geerits, H. Lemmel, A. Berger, and S. Sponar. Phase vortex lattices in neutron interferometry. *Nat. Comm. Phys*, 6:209, 2023.
- [16] R. Cappelletti, T. Jach, and J. Vinson. Intrinsic orbital angular momentum states of neutrons. *Phys. Rev. Lett.*, 120:090402, 2018.
- [17] Wolfgang Treimer, Frank Haußer, and Martin Suda. On the neutron orbital angular momentum: Has it actually been demonstrated? *Arxiv*, page 2309.03594v1, 2023.
- [18] A.V. Afanasev, D.V. Karlovets, and V.G. Serbo. Schwinger scattering of twisted neutrons by nuclei. *Phys. Rev. C*, 100:051601, 2019.
- [19] A.V. Afanasev, D.V. Karlovets, and V.G. Serbo. Elastic scattering of twisted neutrons by nuclei. *Phys. Rev. C*, 103:054612, 2021.
- [20] T. Jach and J. Vinson. Method for the definitive detection of orbital angular momentum states in neutrons by spin-polarized  $^3\text{He}$ . *Phys. Rev. C*, 105:L061601, 2022.
- [21] J. Courtial, K. Dholakia, D. A. Robertson, L. Allen, and M. J. Padgett. Measurement of the rotational frequency shift imparted to a rotating light beam possessing orbital angular momentum. *Phys. Rev. Lett.*, 80:3217–3219, 1998.
- [22] H. Rauch, H. Wolwitsch, H. Kaiser, R. Clothier, and S. A. Werner. Measurement and characterization of the three-dimensional coherence function in neutron interferometry. *Phys. Rev. A*, 53:902–908, 1996.
- [23] Apoorva G. Wagh, Sohrab Abbas, and Wolfgang Treimer. The plain truth about forming a plane wave of neutrons. *Nuclear Instruments and Methods in Physics Research Section A: Accelerators, Spectrometers, Detectors and Associated Equipment*, 634:S41–S45, 2011.
- [24] S. McKay, A. A. M. Irfan, Q. Le Thien, N. Geerits, S. R. Parnell, R. M. Dalgliesh, N. V. Lavrik, I. I. Kravchenko, G. Ortiz, and R. Pynn. Experimental evidence for the two-path description of neutron spin echo. *Phys. Rev. A*, 109:042420, 2024.
- [25] R. Gaehler, R. Golub, K. Habicht, T. Keller, and J. Felber. Space-time description of neutron spin echo spectrometry. *Physica B*, 229:1–17, 1996.
- [26] Wim G. Bouwman, Chris P. Duif, Jeroen Plomp, Albrecht Wiedenmann, and Roland Gahler. Combined SANS-SESANS, from 1 nm to 0.1 mm in one instrument. *Physica B*, 406:2357–2360, 2011.



- [27] N. Geerits, S. R. Parnell, M. A. Thijs, A. A. van Well, C. Franz, A. L. Washington, D. Raspon, R. M. Dalgliesh, and J. Plomp. Time of flight modulation of intensity by zero effort. *Review of Scientific Instruments*, 90:125101, 2019.
- [28] J. Shen, S.J. Kuhn, R.M. Dalgliesh, V.O. de Haan, N. Geerits, A.A.M. Irfan, F. Li, S. Lu, S.R. Parnell, J. Plomp, A.A. van Well, A. Washington, D.V. Baxter, G. Ortiz, W.M. Snow, and R. Pynn. Unveiling contextual realities by microscopically entangling a neutron. *Nat. Commun.*, 11:930, 2020.
- [29] S. J. Kuhn, S. McKay, J. Shen, N. Geerits, R. M. Dalgliesh, E. Dees, A. A. M. Irfan, F. Li, S. Lu, V. Vangelista, D. V. Baxter, G. Ortiz, S. R. Parnell, W. M. Snow, and R. Pynn. Neutron-state entanglement with overlapping paths. *Phys. Rev. Research*, 3:023227, 2021.
- [30] Victor-O. de Haan, Jeroen Plomp, Ad A. van Well, M. Theo Rekveldt, Yuji H. Hasegawa, Robert M. Dalgliesh, and Nina-Juliane Steinke. Measurement of gravitation-induced quantum interference for neutrons in a spin-echo spectrometer. *Phys. Rev. A*, 89:063611, 2014.
- [31] Robert Dalgliesh, Michael Snow, Victor de Haan, Kyle Steffen, and Niels Geerits. Detection of the sagnac effect in SESANS, 2024. <https://doi.org/10.5286/ISIS.E.RB2410116>.
- [32] M.Theo Rekveldt. Novel sans instrument using neutron spin echo. *Nucl. Inst. and Meth. in Phys. Res. B*, 114:366–370, 1996.
- [33] Fankang Li, Steven R. Parnell, Hongyu Bai, Wencao Yang, William A. Hamilton, Brian B. Maranville, Rana Ashkar, David V. Baxter, J. Ted Cremer, and Roger Pynn. Spin echo modulated small-angle neutron scattering using superconducting magnetic wollaston prisms. *Journal of Applied Crystallography*, 49:55–63, 2016.
- [34] S. R. Parnell, A. A. van Well, J. Plomp, R. M. Dalgliesh, N.-J. Steinke, J. F. K. Cooper, K. E. Steffen N. Geerits, W. M. Snow, and V. O. de Haan. Search for exotic spin-dependent couplings of the neutron with matter using spin-echo based neutron interferometry. *Phys. Rev. D*, 101:122002, 2020.
- [35] G. J. Nilsen, J. Kosata, M. Devonport, P. Galsworthy, R. I. Bewley, D. J. Voneshen, R. Dalgliesh, and J. R. Stewart. Polarisation analysis on the let time-of-flight spectrometer. *Journal of Physics: Conference Series*, 862:012019, 2017.
- [36] G. Cassella, J. R. Stewart, G. M. Patern, V. Garcia Sakai, M. Devonport, P. J. Galsworthy, R. I. Bewley, D. J. Voneshen, D. Raspino, and G. J. Nilsen. Polarization analysis on the LET cold neutron spectrometer using a  $^3\text{He}$  spin-filter: first results. *Journal of Physics: Conference Series*, 1316:012007, 2019.
- [37] S. V. Grigoriev, R. Kreuger, W. H. Kraan, F. M. Mulder, and M. Th. Rekveldt. Neutron wave-interference experiments with adiabatic passage of neutron spin through resonant coils. *Phys. Rev. A*, 64:013614, 2001.
- [38] W.H. Kraan, S.V. Grigoriev, M.Th. Rekveldt, H. Fredrikze, C.F. de Vroege, and J. Plomp. Test of adiabatic spin flippers for application at pulsed neutron sources. *Nuclear Instruments and Methods in Physics Research A*, 510:334–345, 2003.
- [39] J. Leach, M.J. Padgett, S.M. Barnett, S. Franke-Arnold, and J. Courtial. Measuring the orbital angular momentum of a single photon. *Phys. Rev. Lett.*, 88:257901, 2002.
- [40] Raffaele Silvestri, Haocun Yu, Teodor Strömberg, Christopher Hilweg, Robert W. Peterson, and Philip Walther. Experimental observation of earth’s rotation with quantum entanglement. *Science Advances*, 10:eado0215, 2024.